Janus Graphene: Scalable Self#Assembly and Solution#Phase Orthogonal Functionalization

ADVANCED MATERIALS
www.advmat.de

Janus Graphene: Scalable Self-Assembly and Solution-Phase Orthogonal Functionalization

Intak Jeon, Martin D. Peeks, Suchol Savagatrup, Lukas Zeininger, Sehoon Chang, Gawain Thomas, Wei Wang, and Timothy M. Swager*

Orthogonal functionalization of 2D materials by selective assembly at interfaces provides opportunities to create new materials with transformative properties. Challenges remain in realizing controllable, scalable surface-selective and orthogonal functionalization. Herein, dynamic covalent assembly is reported that directs the functionalization of graphene surfaces at liquid–liquid interfaces. This process allows for facile addition and segregation of chemical functionalities to impart Janus characteristics to graphenes. Specifically, the dynamic covalent functionalization is accomplished via Meisenheimer complexes produced by reactions of primary amines with pendant dinitroaromatics attached to graphenes. Janus graphenes are demonstrated to be powerful surfactants that organize at water/organic, water/fluorocarbon, and organic/fluorocarbon liquid interfaces. This approach provides general access to the creation of diverse surfactant materials and promising building blocks for 2D materials.

Multifunctional materials that leverage anisotropic intermolecular interactions find many useful applications in biomedical, sensing, and morphological templating.[1–9] For example, polymers with two asymmetric functional groups displaying preferential orientations at the air–water interface allow for precise presentation of chemical features, depending on the affinity of functional groups.[10] We have targeted disc-shaped Janus objects that display remarkable stabilization at oil–water interfaces.[11] In this context, graphenes have the potential for asymmetric functionalization on its surfaces. However, orthogonal functionalization of the two basal planes of graphene sheets remains a challenge and 2D Janus graphene (JG) architectures are rare.[12–19] Herein we report a highly controllable, scalable and versatile strategy for the fabrication of 2D Janus graphene nanosheets via dynamic covalent functionalization of a functionalized graphene precursor at the liquid–liquid interface. We demonstrate the utility of 2D JG for oil recovery as Pickering emulsifiers, potential membrane precursors, and for the stabilization of complex interfaces.

The interfacial trapping and lateral self-assembly of 3,5-dinitrophenyl functionalized graphenes (FGs) at the ethyl acetate–water interface affords the opportunity to explore differential functionalization at interfaces to create 2D JGs (**Figure 1**a). The FG has 3,5-dinitrophenyl groups on the π-conjugated surfaces of both basal planes that reduce intersheet interactions and stacking, in contrast to the strong π–π attractions between pristine graphene sheets (Figure S1, Supporting Information).[20] This allows individual sheets of FGs in 2D assemblies to simultaneously interact with two different liquids at an interface (Figure 1a). Once organized at an interface, the anisotropic disc-like FGs (width/thickness ratio ≈40) experience attractive capillary interactions, leading to laterally edge-packed structures (Figure 1b).[20,21] This organization allows for the controllable functionalization with linear hydrocarbon, fluorocarbon, and/or water-soluble-ethylene oxide chains of the two separate FG surfaces to produce JGs (Figure 1c). The functionalization is accomplished by amine addition to the electron deficient 3,5-dinitrophenyl groups on the graphene basal planes. The resulting connections involve reversible covalent bonds through Meisenheimer complexes formation, which occurs at liquid–liquid interfaces. We confirm the asymmetric nature and functionalization of the JGs by interfacial studies and spectroscopic methods.

Figure 2 and Figure S2 (Supporting Information) illustrate the 2D assembly of FG at the liquid–liquid interface for various solvent pairs. During the agitation of liquids with FGs, FGs are trapped with the kinetic adsorption of air at the water–organic interface (Figure 2a). This mechanism depends on the ability of the FG and air to competitively adsorb at the interface, which is related to the liquid–air interfacial tension (Figure 2b). Trapped air is relatively energetically unfavorable and FG decreases the free energy of the system, resulting in its assembly at the

Dr. I. Jeon, Dr. M. D. Peeks, Dr. S. Savagatrup, Prof. T. M. Swager
Department of Chemistry
Institute for Soldier Nanotechnologies
Massachusetts Institute of Technology
Cambridge, MA 02139, USA
E-mail: tswager@mit.edu
Dr. L. Zeininger
Department of Chemistry
Massachusetts Institute of Technology
Cambridge, MA 02139, USA
Dr. S. Chang, G. Thomas, Dr. W. Wang
Aramco Services Company
Aramco Research Center-Boston
Cambridge, MA 02139, USA
The ORCID identification number(s) for the author(s) of this article can be found under https://doi.org/10.1002/adma.201900438.

DOI: 10.1002/adma.201900438

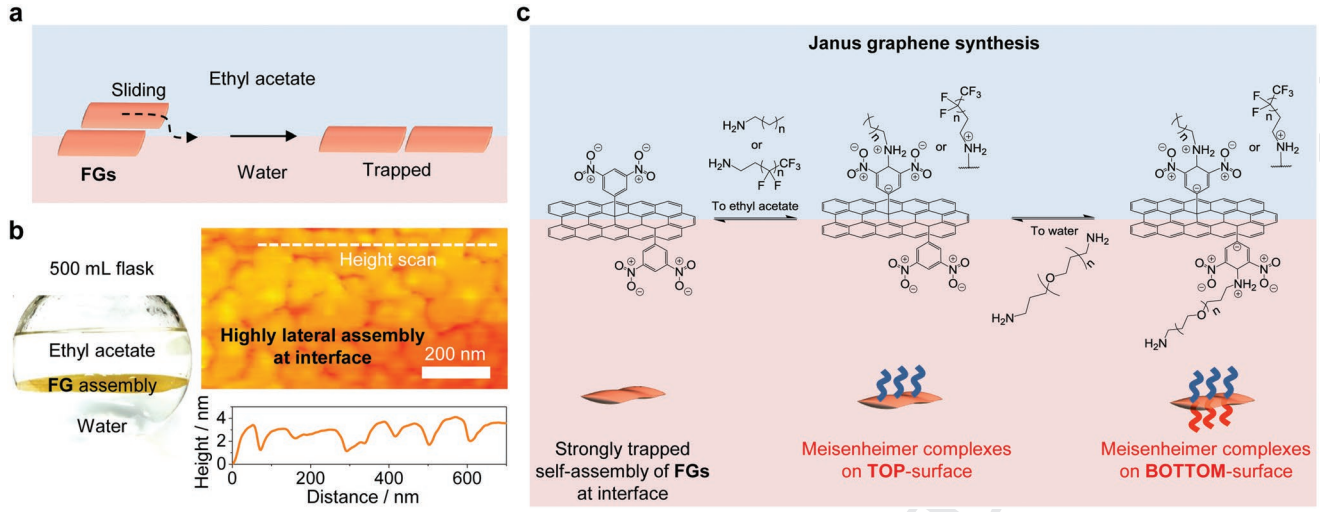

Figure 1. Self-assembly of FGs and JG synthesis at interface. a) An assembly of individualized FG sheets forms at the ethyl acetate–water interface, as a result of the high density of 3,5-dinitrophenyl groups on the π-conjugated surfaces that significantly reduce interlayer stacking. b) Left: a photograph of the large area FG assembly in a 500 mL flask. Right: atomic force microscopy (AFM) topology of the FG assembly that was lifted from the liquid interface onto a mica substrate. c) Synthetic procedure for the preparation of 2D **JG** using orthogonal Meisenheimer complex formation on interfacially trapped FG with 3,5-dinitrophenyl groups.

liquid–liquid interface. The trapping efficiency of FGs depends on the energy contribution of air at the interface of immiscible liquids, as can be briefly expressed by[22–24]

$$\text{FG trapping efficiency} \propto \gamma_{w\text{–}a} - \gamma_{s\text{–}a} - \gamma_{w\text{–}s} \quad (1)$$

where $\gamma_{w\text{–}a}$, $\gamma_{s\text{–}a}$, and $\gamma_{w\text{–}s}$ are interfacial tension of water–air, solvent–air, and water–solvent, respectively.[25–27] Although the interfacial tension of FG-liquid is excluded, air dominantly contributes to the interfacial trapping efficiency. The water–ethyl acetate system shows the most unfavorable interfacial adsorption of air and thereby affords a high interfacial area for the assembly of materials (Figure 2b). As a result, FG is most effectively trapped at the interface of the immiscible combination of ethyl acetate and water (Movie S1, Supporting Information). The FG assembly decreases the ethyl acetate–water interfacial tension to a value of 6.33 mN m^{-1} at 21 °C, measured by the Du Noüy ring method. According to Binks' analysis, the free energy of detachment (ΔG_{dw}) of a disc-like FG (width/thickness ratio ≈40) into water is expressed by[28–31]

$$\Delta G_{dw} = \gamma_{w\text{–}s}\pi b^2(1-\cos\theta)^2 \times (\text{aspect ratio dependency}) \quad (2)$$

where θ is the three-phase contact angle with the disc-like particle, and b is the length of the disc-like particle in its minor (short) semi-axis. The FG is 2.4 nm thick and the disc-like FG is expected to be strongly trapped at the interface ($\Delta G_{dw} \gg k_B T$). The assembly of FG has a face-on structure that orients with each side-facing opposite liquid interfaces (Figure 1b). Alternatively, if air is competitive for the interface as in Case 2, kinetically trapped air reduces the efficiency of the interfacial trapping of FGs at the interface. The partitioning of carbon materials in mixed solvents depends on their solubility or dispersibility (Figure 2d). Graphene, reduced graphene oxide (rGO), and unfunctionalized carbon nanotubes (CNT) all lack strong interactions with solvents and therefore can also be trapped at an ethyl acetate–water interface. However, these carbon nanomaterials randomly aggregate as a result of their strong π–π interactions. Other materials are strongly dissolved and dispersed in solvents. For example, water-soluble graphene oxide (GO) with dense oxygenated groups, cannot be organized at these interfaces. Thus, FG with greatly reduced sheet-to-sheet interactions organizes into equilibrium structures at interfaces and can be reactively converted into a Janus structure.

Hansen solubility parameters (Table S1, Supporting Information) provide an intuitive tool for the selection of compatible solvents for interfacial trapping of carbon nanotube and graphene dispersions.[32,33] We successfully selected solvents that concentrate FG at their interfaces with water.[34] Appropriate solvents for interfacial trapping have 14.5 MPa$^{0.5}$ < δ_D < 15.8 MPa$^{0.5}$, 2.9 MPa$^{0.5}$ < δ_P < 8.4 MPa$^{0.5}$ and 3.5 MPa$^{0.5}$ < δ_H < 10.2 MPa$^{0.5}$, where δ_D, δ_P, and δ_H are the dispersive, polar, and hydrogen bonding solubility parameters (Figure 2d). As expected, the ethyl acetate–water combination is the most effective system. Our findings show that FG assembles into a well-defined film at the liquid–liquid interface when three requirements are met: i) Two liquids must be largely immiscible to generate an interface. ii) The solvents must only weakly solvate the graphenes. FG, rGOs, CNTs, and graphenes occupy the interface of water and ethyl acetate, whereas fully solvated GOs have too great an affinity for the bulk water. iii) The solvents need to have lower interfacial tension with water than with air. For example, solvents containing hydrogen bonding acetate ester (CH_3CO_2–R) and ether (R–O–R′) groups cause FG to assemble at the organic–water interface. To transport the FG from the bulk phase to the liquid–liquid interface requires the external mechanical force that breaks the two immiscible liquid phases into emulsion droplets with FG separating the two liquids (Figure S3a, Supporting Information). During agitation, the FG quickly moves to the water–ethyl acetate interface by Rayleigh-Bénard convection (Figure S3a, Supporting Information).[35] Finally, at equilibrium, the FG is preferentially adsorbed at the

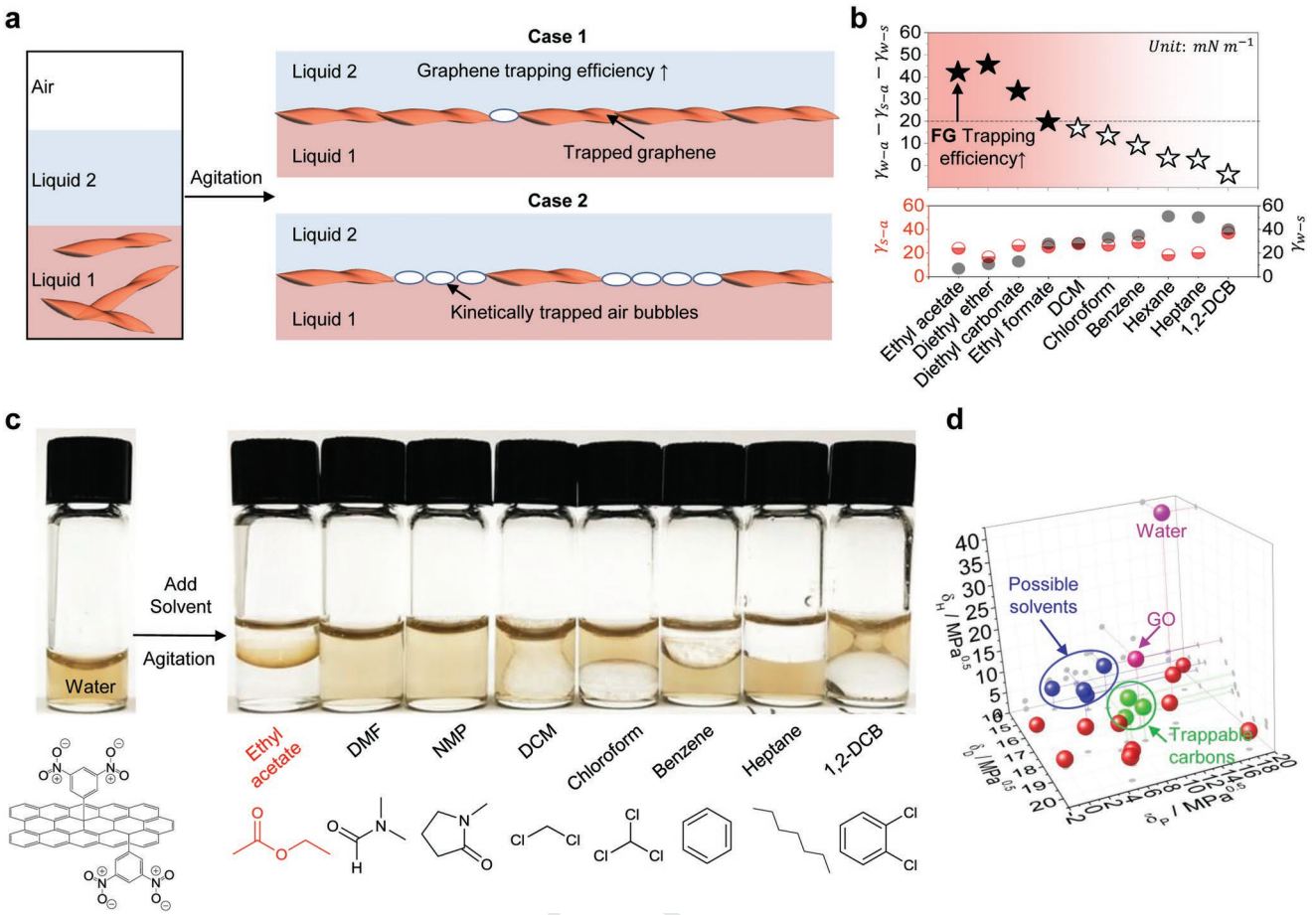

Figure 2. Interfacial trapping of FGs at the agitated liquid interface. a) Graphenes assemble in an agitated immiscible Liquid–Liquid solution with interfacial trapping at the interface. In Case 1 with Liquid 1–Liquid 2, graphene is energetically driven to occupy effectively all of the liquid–liquid interface. For Case 2, it is energetically favorable for both graphene and air to occupy the interface of an immiscible Liquid 1–Liquid 2 interface. b) Summary of the interfacial tensions of various liquid–air systems. c) FGs are dispersed in the water phase and each solvent is added and then mixed. FGs assemble as a film only at the interface of ethyl acetate/water system. In the other cases, the FG persists in the water phase. d) Hansen solubility parameters plot for solvents as a function of dispersive (δ_D), polar (δ_P), and hydrogen bonding (δ_H) interactions. Water-immiscible solvents within the blue circle cause FGs to localize at the interface. Green dots represent: graphene, reduced graphene oxide (rGO), and unfunctionalized carbon nanotube (CNT). The high degree of oxygen functionality in GO results in strong H-bonding interactions with water, and trapped GOs are not observed at the interface.

water–ethyl acetate interface. At a transient stage, the FG and air bubbles both encapsulate water at the interface (Figure S3b and Movie S2, Supporting Information). Then the FG assembles, the air bubbles collapse, and the encapsulated water joins the bulk water. The strongly interfacially trapped FG moves with the interface while the weakly trapped air layer remains at the initial position. In case of a low-density assembly of FG, the addition of a rhodamine B dye induces a gradient of the interfacial tension at the interface that rearranges the assembly of FG and air bubbles (Figure S3c and Movie S3, Supporting Information). The results are consistent with the interfacial trapping of FG in a water–ethyl acetate–kinetically trapped air system. When the concentration of FG is high enough, it fully saturates the interface and reaches the critical interfacial concentration for stable Pickering emulsion formation (Figure S3d, Supporting Information).

Once the FG assemblies are trapped at an interface, they can then be reacted to produce Meisenheimer complexes with *n*-octylamine (H) or 1*H*,1*H*,2*H*,2*H*-perfluorooctylamine (F) in ethyl acetate, and 4,7,10-trioxa-1,13-tridecanediamine (W) chains in water (**Figure 3**a and Figure S4, Supporting Information). After the H or F chains in ethyl acetate phase add to the surface, they tightly anchor FG at the interface (Figure 3b and Figure S5, Supporting Information). Subsequently, water-soluble linear W chains are added into the water phase so that the FG surface facing the water can also be functionalized through Meisenheimer complexes formation (Figure 3c). As the glass of the vial is hydrophilic, driven by Marangoni force, the hydrophilic surface of the JG climbs the wall spreading the hydrophobic surface of the mixed ethyl acetate-hexane solution (Figure 3d and Movie S4, Supporting Information). Most importantly, nearly all JGs continued to remain at the interface, indicating a strong adsorption at the interface. Notably, the well-defined and orthogonally functionalized JGs are efficiently trapped and their basal planes are self-assembled at the interface. The persistent structure at the interface enables sequential chemical modifications with the graphene surfaces facing the water being functionalized with ethylene oxide groups and the surfaces facing the organic

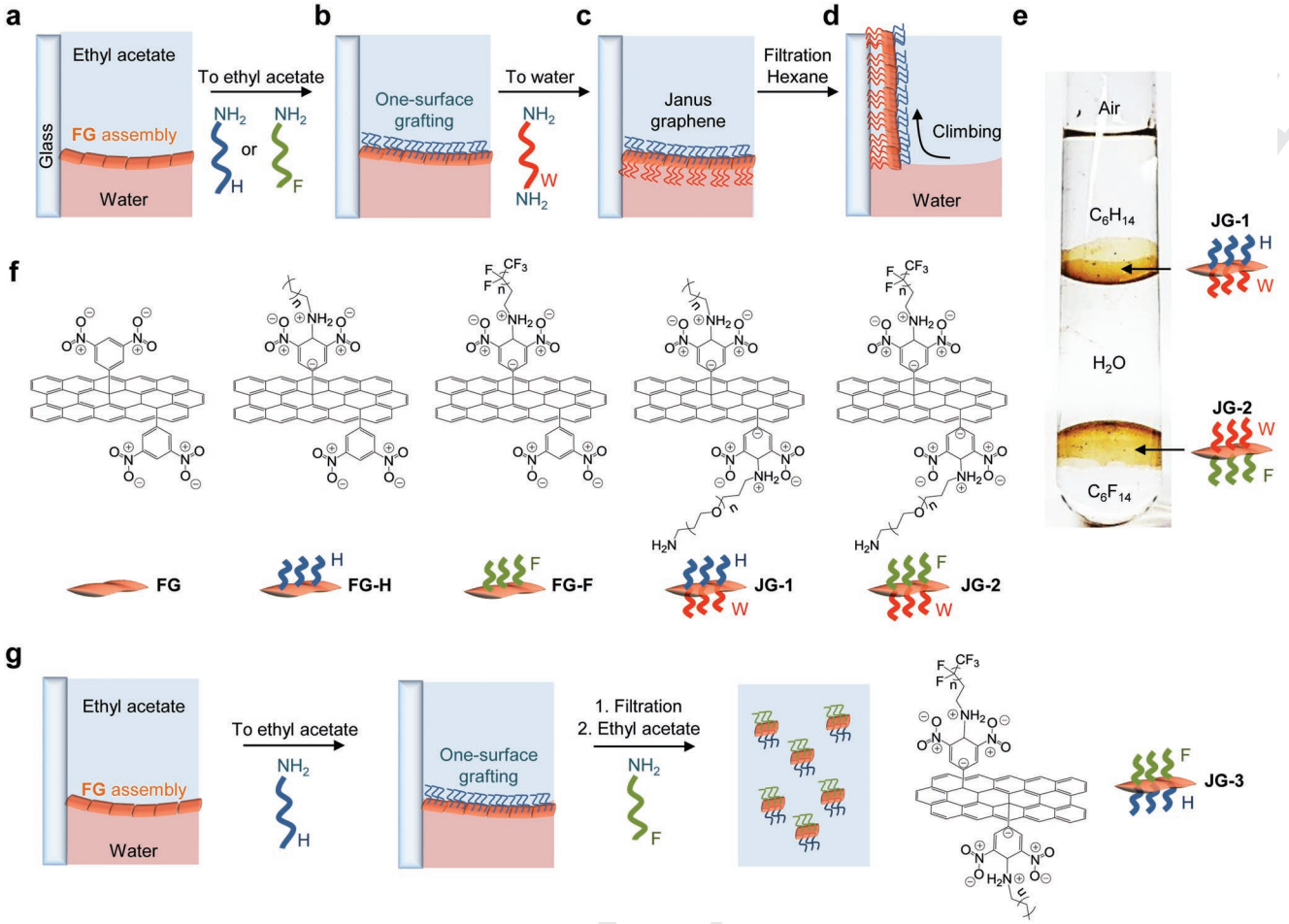

Figure 3. Schematic of the procedure to create FG-H, FG-F, JG-1, JG-2, and JG-3. a) FG adsorbs at the interface of ethyl acetate and water. b) Linear H or F chains functionalize the upper surface of the FG at the interface to create FG-H and FG-F, respectively. c) JG-1 or JG-2 is formed by the addition of linear water-soluble W chains to the water phase. The functional groups are bound by Meisenheimer complex formation that occurs on each of the graphene surfaces. The graphenes have two different chemical functionalities and stabilize immiscible liquid–liquid interfaces with complementary character. d) JG-1 climbs the hydrophilic glass wall of vials in mixed ethyl acetate–hexane–water system. e) JG-1 and JG-2 are trapped in the water–hexane and water–perfluorohexane interfaces, respectively. f) Chemical structures of FG, FG-H, FG-F, JG-1, and JG-2. g) Schematic procedure for the creation of JG-3 by first isolating FG-H and then functionalizing in ethyl acetate with F chains.

phase being functionalized separately (Figure 3e,f). JG-3 can be produced by a similar method as in Figure 3g. The FG starting material has an average thickness of 2.4 ± 0.2 nm with an mean lateral area of 0.012 μm^2 as determined by transmission electron microscopy (TEM) and atomic force microscope (AFM) measurements (Figures S6 and S7, Supporting Information). The average AFM heights of FG-H and JG-1 are found to be 3.4 ± 0.4 nm and 4.7 ± 0.4 nm, respectively. These thickness measurements show that the stepwise surface-selective orthogonal functionalization on graphenes is easily achieved through our method. As a further support for the successful formation of JGs or single surface grafting through interfacial trapping and Meisenheimer complexes, we performed diffusion-ordered NMR spectroscopy (NMR 1*H* DOSY), attenuated total reflectance-Fourier transform infrared spectroscopy (ATR-FTIR), and X-ray photoelectron spectroscopy (XPS) analysis (Figures S8 and S9, Supporting Information). From NMR 1*H* DOSY, we observed the H and W groups to be attached to the slowly diffusing graphenes. The asymmetrical functionalities on the two surfaces of the nanometer thick JGs create powerful new surfactant 2D materials for interfacial chemistry and biology.

The Janus graphenes with two chemically different compartments show unique activities at liquid interfaces. First, JG-1 climbs the walls of a glass vial as a result of a high-energy interface created by a thin layer of water on the hydrophilic glass in contact with the hexane to minimizing the interfacial energy (**Figure 4**a and Movie S4, Supporting Information). We can induce nonspherical emulsions with kinetically jammed JG-1**s** by the restriction of equilibrium shapes (Figure 4a).[36] When the total area of JG-1 surfactants oversaturates the area of the liquid interface ($\sum A_{JG-1} > A_{Interface}$), jammed assembly of JG-1 arrests the nonequilibrium shapes of hexane in water. JG-1 with orthogonally distinguishable hydrophobic and hydrophilic surfaces follows the rules for the interactions of the menisci: similar menisci attract and dissimilar menisci repel.[37] Thermodynamics drives JG-1 to assemble into a continuous structure, and such processes have potential utility in the production of barrier or membrane structures. Water droplets added through

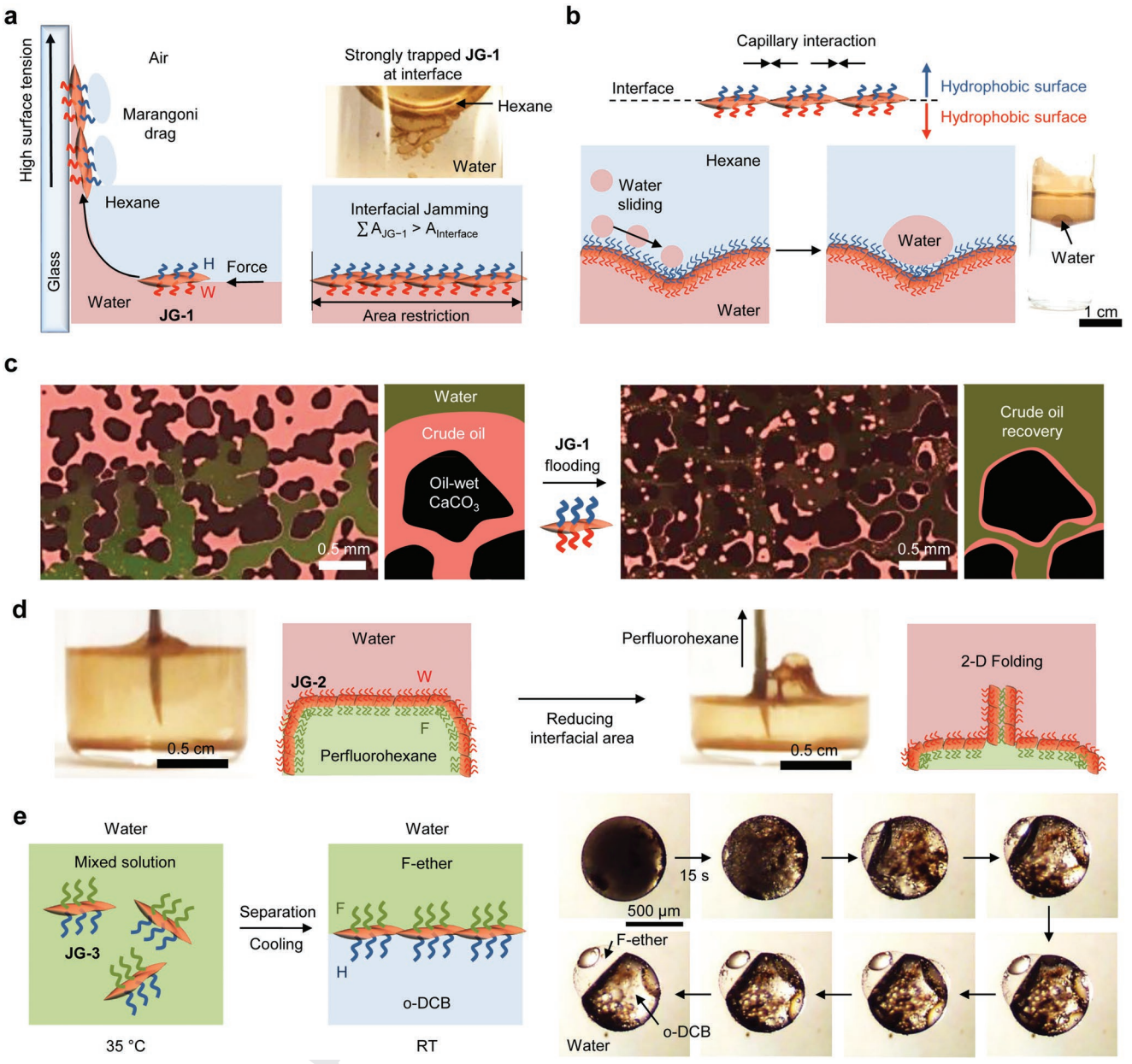

Figure 4. Applications of JGs. a) Left: JG-1 climbs along the glass vial surface from the water–hexane interface to the air–glass interface with hexane through Marangoni flow. Right: the interfacial jamming of the JG-1 surfactants is observed. b) The attractive capillary interactions are expected such that the structure is connected and forms a dense edge–edge assembly. Water droplets slide on the hydrophobic surface of the 2D JG-1 assembly. The assembly of JG-1 at the interface supports a coalesced water droplet. c) 2D JG-1 injection in the microfluidic system that emulates oil in a carbonate mineral formation. Left: After water (green-dyed) flooding, 39 ± 2% (determined by image processing) of crude oil (red) remained. Right: After a JG-1 water solution flooding, 25 ± 1% of crude oil remained, indicating enhanced oil removal. d) When the density of JG-2 at the interface reaches the critical concentration, the JG-2 experiences an attractive force and forms bilayer assembly above the interface. e) At elevated temperature 35 °C above T_c, *1,2*-DCB and F-ether with JG-3 are miscible and emulsified in aqueous 0.1% Zonyl FS-300 and 0.1% sodium dodecyl sulfate. Below T_c, the mixed phase separates to create a Janus droplet in water. During cooling, JG-3 moves to the *1,2*-DCB and F-ether interface.

the nonaqueous phase slide freely on the hydrophobic assembled graphene surface and are supported by this dense JG-1 assembly (Figure 4b). The graphene layer prevents the water droplet from coalescing with the bottom water reservoir, confirming that the added water is segregated by a mechanically robust hydrophobic surface. Janus graphene can also be used as a chemical-enhanced oil recovery (CEOR) reagent. To demonstrate usage of JG-1 in CEOR applications, we used a microfluidic-based reservoir model to understand oil-water-rock phase interactions and visualize the fluid transport processes in micropores (Figure S10, Supporting Information).[38] Figure 4c shows the oil distribution after flooding the micropores using water with JG-1 (91 μg mL^{-1}). In the presence of JG-1, a 14% improvement in oil recovery was observed compared to pure

water (Figure 4c and Figure S11, Supporting Information).[13] The result illustrates the opportunity for functionalized Janus 2D surfactants to be utilized for extraction of organics from water and oil recovery applications.

We further observe surfactant-like interfacial phenomena of the JG-2 layer when its surface density increases (Figure 4d). At high interfacial density of JG-2, the layer becomes unstable and then folds to form a bilayer, or 3-D aggregates. Figure 4d and Movie S5 (Supporting Information) show bi-layer formation: folding, growth and collapsing. It is similar to the way that micelles or lipids form in a bulk phase above the critical micelle concentration.[39] Figure 4e and Movie S6 (Supporting Information) illustrate the rearrangement for JG-3 that is trapped at the *1,2*-dichlorobenzene (*1,2*-DCB)/ethyl nonafluorobutyl ether (F-ether) interface. To validate whether JG-3 behaves as a surfactant at the interface of hydrocarbon and fluorocarbon liquids, we used complex liquids that can convert into Janus configurations (Figure S12, Supporting Information).[40] In the initial stage at 35 °C, JG-3 is dispersed in the single phase of *1,2*-DCB/F-ether. During cooling below the upper consolute temperature (T_c), phase separation of the *1,2*-DCB and F-ether occurs within the dispersed water droplets. The JG-3 then localizes at the *1,2*-DCB/F-ether interface in the Janus droplet configuration (Figure S13, Supporting Information), and these droplets show a lower T_c than those without JG-3. These effects demonstrate the affinity of JG-3 to both the hydrocarbon and fluorocarbon phases.

In summary, we have reported a method for synthesis of various JGs with different functionalities that is general, scalable, and provides new possibilities in interfacial chemistry. Fully occupied and trapped graphenes at immiscible interfaces of water and ethyl acetate enable each surface to react with distinct chemical functions through Meisenheimer complex formation. In principle, various functional pairs can be covalently bonded onto each surface of graphene to create a wide diversity of JGs. When cografting different chemical functions on each side of graphene, each surface faces different liquid environments and the activity of JGs modifies the interface of liquids. In principle, this synthetic strategy toward JGs can be extended to other 2D solid materials: **graphenes**, FGs, rGOs, functionalized GOs, CNTs, MoS_2, and 2D metal–organic frameworks. 2D tailored JGs enable functional hierarchical structures of interest to molecular biology and medicinal chemistry.

Supporting Information

Supporting Information is available from the Wiley Online Library or from the author.

Acknowledgements

I.J. and T.M.S. developed the concept for the research. I.J. designed the synthesis method for Janus graphenes, performed measurements, and analyzed the data in the paper. I.J., M.D.P., S.S., and L.Z. conducted experiments involving emulsion fabrication, imaging, and NMR studies. S.C., G.T., and W.W., conducted oil recovery test. I.J. and T.M.S. wrote, and all authors commented on, the manuscript. The authors thank Dr. M. He for the synthesis of 3,5-dinitrobenzenediazonium salts, G. Park at MIT Bio-instrumentation Lab (Prof. I. Hunter) for high speed camera measurements, and Dr W. W. Massefski for helpful discussions. M.D.P. thanks the English-Speaking Union for a Lindemann Trust Fellowship. S.S. was supported by an F32 Ruth L. Kirschstein National Research Service Award. L.Z. acknowledges support from the German Research Foundation (DFG, Grant No. ZE1121/1-1). The authors also thank the Institute for Soldier Nanotechnologies at MIT for use of equipment.

Conflict of Interest

The authors declare no conflict of interest.

Keywords

graphene, interfacial arrangement, interfacial trapping, Janus, self-assembly

Received: January 19, 2019
Revised: March 11, 2019
Published online:

[1] I. Bita, J. K. W. Yang, Y. S. Jung, C. A. Ross, E. L. Thomas, K. K. Berggren, *Science* **2008**, *321*, 939.
[2] E. Kopperger, J. List, S. Madhira, F. Rothfischer, D. C. Lamb, F. C. Simmel, *Science* **2018**, *359*, 296.
[3] H. Qiu, Z. M. Hudson, M. A. Winnik, I. Manners, *Science* **2015**, *347*, 1329.
[4] L. L. Ong, N. Hanikel, O. K. Yaghi, C. Grun, M. T. Strauss, P. Bron, J. Lai-Kee-Him, F. Schueder, B. Wang, P. F. Wang, J. Y. Kishi, C. Myhrvold, A. Zhu, R. Jungmann, G. Bellot, Y. G. Ke, P. Yin, *Nature* **2017**, *552*, 72.
[5] K. H. Roh, D. C. Martin, J. Lahann, *Nat. Mater.* **2005**, *4*, 759.
[6] X. M. Mao, Q. Chen, S. Granick, *Nat. Mater.* **2013**, *12*, 217.
[7] Y. F. Wang, Y. Wang, D. R. Breed, V. N. Manoharan, L. Feng, A. D. Hollingsworth, M. Weck, D. J. Pine, *Nature* **2012**, *491*, 51.
[8] S. Sacanna, M. Korpics, K. Rodriguez, L. Colon-Melendez, S. H. Kim, D. J. Pine, G. R. Yi, *Nat. Commun.* **2013**, *4*, 1688.
[9] G. Singh, H. Chan, A. Baskin, E. Gelman, N. Repnin, P. Kral, R. Klajn, *Science* **2014**, *345*, 1149.
[10] J. Kim, T. M. Swager, *Nature* **2001**, *411*, 1030.
[11] Y. Nonomura, S. Komura, K. Tsujii, *Langmuir* **2004**, *20*, 11821.
[12] L. M. Zhang, J. W. Yu, M. M. Yang, Q. Xie, H. L. Peng, Z. F. Liu, *Nat. Commun.* **2013**, *4*, 1443.
[13] D. Luo, F. Wang, J. Y. Zhu, F. Cao, Y. Liu, X. G. Li, R. C. Willson, Z. Z. Yang, C. W. Chu, Z. F. Ren, *Proc. Natl. Acad. Sci. USA* **2016**, *113*, 7711.
[14] D. S. Yu, E. Nagelli, R. Naik, L. M. Dai, *Angew. Chem., Int. Ed.* **2011**, *50*, 6575.
[15] B. T. McGrail, J. D. Mangadlao, B. J. Rodier, J. Swisher, R. Advincula, E. Pentzer, *Chem. Commun.* **2016**, *52*, 288.
[16] Y. F. Yang, L. Zhang, X. T. Ji, L. X. Zhang, H. F. Wang, H. Y. Zhao, *Macromol. Rapid Commun.* **2016**, *37*, 1520.
[17] H. Wu, W. Y. Yi, Z. Chen, H. T. Wang, Q. G. Du, *Carbon* **2015**, *93*, 473.
[18] A. de Leon, B. J. Rodier, Q. M. Luo, C. M. Hemmingsen, P. R. Wei, K. Abbasi, R. Advincula, E. B. Pentzer, *ACS Nano* **2017**, *11*, 7485.
[19] A. Holm, J. Park, E. D. Goodman, J. M. Zhang, R. Sinclair, M. Cargnello, C. W. Frank, *Chem. Mater.* **2018**, *30*, 2084.

[20] I. Jeon, B. Yoon, M. He, T. M. Swager, *Adv. Mater.* **2018**, *30*, 1704538.
[21] P. J. Yunker, T. Still, M. A. Lohr, A. G. Yodh, *Nature* **2011**, *476*, 308.
[22] S. Sacanna, W. K. Kegel, A. P. Philipse, *Phys. Rev. Lett.* **2007**, *98*, 158301.
[23] E. Vignati, R. Piazza, T. P. Lockhart, *Langmuir* **2003**, *19*, 6650.
[24] R. McGorty, J. Fung, D. Kaz, V. N. Manoharan, *Mater. Today* **2010**, *13*, 34.
[25] J. J. Jasper, *J. Phys. Chem. Ref. Data* **1972**, *1*, 841.
[26] A. H. Demond, A. S. Lindner, *Environ. Sci. Technol.* **1993**, *27*, 2318.
[27] Y. Lin, H. Skaff, T. Emrick, A. D. Dinsmore, T. P. Russell, *Science* **2003**, *299*, 226.
[28] B. P. Binks, T. S. Horozov, *Colloidal Particles at Liquid Interfaces*, Cambridge University Press, Cambridge **2006**.
[29] K. S. Kim, Y. Zhao, H. Jang, S. Y. Lee, J. M. Kim, K. S. Kim, J. H. Ahn, P. Kim, J. Y. Choi, B. H. Hong, *Nature* **2009**, *457*, 706.
[30] X. L. Li, G. Y. Zhang, X. D. Bai, X. M. Sun, X. R. Wang, E. Wang, H. J. Dai, *Nat. Nanotechnol.* **2008**, *3*, 538.
[31] J. Kim, L. J. Cote, F. Kim, W. Yuan, K. R. Shull, J. X. Huang, *J. Am. Chem. Soc.* **2010**, *132*, 8180.
[32] C. M. Hansen, *Hansen Solubility Parameters: A User's Handbook*, CRC Press, Boca Raton, FL **2007**.
[33] Y. Hernandez, M. Lotya, D. Rickard, S. D. Bergin, J. N. Coleman, *Langmuir* **2010**, *26*, 3208.
[34] J. N. Coleman, *Acc. Chem. Res.* **2013**, *46*, 14.
[35] J. Shim, J. M. Yun, T. Yun, P. Kim, K. E. Lee, W. J. Lee, R. Ryoo, D. J. Pine, G. R. Yi, S. O. Kim, *Nano Lett.* **2014**, *14*, 1388.
[36] M. M. Cui, T. Emrick, T. P. Russell, *Science* **2013**, *342*, 460.
[37] N. Bowden, F. Arias, T. Deng, G. M. Whitesides, *Langmuir* **2001**, *17*, 1757.
[38] W. Wang, S. Chang, A. Gizzatov, *ACS Appl. Mater. Interfaces* **2017**, *9*, 29380.
[39] H. E. Ries, *Nature* **1979**, *281*, 287.
[40] L. D. Zarzar, V. Sresht, E. M. Sletten, J. A. Kalow, D. Blankschtein, T. M. Swager, *Nature* **2015**, *518*, 520.

